scientific reports

Check for updates

OPEN

Synthesization of metal based-HAP catalysts for enhanced biodiesel yield from palm fatty acid distillate (PFAD)

Nur Athirah Adzahar[1], Abdulkareem Ghassan Abdulkreem Alsultan[1,2,5]✉, Naeemah A. Ibrahim[1,5], Syazana Amira Md. Shahar[1] & Taufiq Yap Yun Hin[1,2,3,4]✉

Biodiesel is a promising alternative fuel and one of the fundamental renewable energy resources due to its unique properties such as significant reduction in greenhouse gas emissions, non-sulfur emissions, non- particulate matter pollutants, low toxicity, and biodegradable. However, it is expensive to produce biodiesel compared to diesel fuel due to the expensive raw material. Heterogeneous catalyst was used because it low cost and easy to separate the product. In this study, biodiesel is studied using high free fatty acid (FFA) feedstock which is palm fatty acid distillate (PFAD) and using different metal-hydroxyapatite (HAP) catalysts; Mg/HAP, Na/HAP, and Cu/HAP. HAP has ion-exchange ability, acid base adjustability and non-toxicity. The catalysts were characterized via X-ray diffraction (XRD), thermogravimetric analysis (TGA), Brunauer-Emmett- Teller surface area measurement (BET), temperature-programmed desorption of ammonia (TPD-NH_3), and the biodiesel was identified using Fourier transform infrared spectroscopy (FTIR) and gas chromatography with flame-ionization detector (GC-FID). The optimum parameter used were molar ratio 10:1 methanol to PFAD within 2 h reaction time at 65 °C. The results showed that only Cu/HAP catalyst works on PFAD to convert to biodiesel due to mesoporous structure as observed in BET, and the biodiesel yield was 40.4%. This might due to presence of strong acid sites that been observed using TPD-NH_3.

In recent decades, the phenomenon of global warming has emerged as a significant concern. Global warming defines as the scientific phenomenon characterized by the increase in the Earth's temperature [1]. For several years, the consumption of fossil fuels has been on the rise due to population growth, leading to greenhouse effects. The combustion of fossil fuels leads to an increase in greenhouse gases, including carbon dioxide, methane, and nitrogen oxide, in the atmosphere[2]. The ongoing global warming, driven by the persistent emission of harmful gases from transportation, has led to significant advancements in green chemistry techniques aimed at reducing pollution. Green chemistry outlines as encompasses the strategy, advancement, and implementation of chemical products and processes aimed at minimizing resource consumption, reducing waste, and enhancing worker safety[3]. As global warming emerges as a critical issue worldwide, there is an increasing emphasis among scientists to concentrate on investigations that incorporate the principles of green chemistry. Green chemistry presents a unique opportunity for the advancement of innovative research publications focused on the development of alternative green and sustainable technologies.

Biodiesel is a prominent green chemistry initiative that has been gaining traction over the past several years as a substitute for fossil fuel consumption. A limited amount of experimental data has been reported regarding the implementation of green chemistry standards in biodiesel production[4]. Therefore, biodiesel serves as a renewable energy source among alternative fuels. Biodiesel, also known as fatty acid methyl ester (FAME), is a renewable and biodegradable fuel. It is a sustainable diesel that can be produced from vegetable oil or animal fat through a transesterification reaction. Biodiesel has emerged as a leading renewable energy

[1]Catalysis Science and Technology Research Centre, Faculty of Science, Universiti Putra Malaysia, UPM, Serdang 43400, Selangor, Malaysia. [2]Department of Chemistry, Faculty of Science, Universiti Putra Malaysia, UPM, Serdang 43400, Selangor, Malaysia. [3]Biomass Valorization and Biomass Energy (BVBE), Catalysis Science and Technology Research Centre, Faculty of Science, Universiti Putra Malaysia, UPM, Serdang 43400, Selangor, Malaysia. [4]University International MAIWP, Taman Batu Muda, Batu Caves, Kuala Lumpur 68100, Malaysia. [5]Fuel and Energy Techniques Eng. Department, South Technical university, Al-Zubair Street, Basra, Iraq. ✉email: kreem.alsultan@yahoo.com; taufiq@upm.edu.my

source and a safe alternative fuel, as it has the potential to reduce global warming, environmental pollution, and dependence on fossil fuels. Biodiesel is widely recognized for its environmental benefits, including renewability and biodegradability, making it an exceptional and sustainable alternative. Biodiesel exhibits comparable physicochemical characteristics to petroleum-based diesel fuel, while also demonstrating superior physical and chemical properties. Biodiesel exhibits a higher flash point and cetane number, lower sulfur content, enhanced lubricity, improved biodegradability, and a minimal carbon footprint[5].

Biodiesel serves as a fuel in diesel engines, also referred to as compression-ignition engines, similar to petroleum-based biodiesel. The mixture of biodiesel, like B20, can influence its performance in various weather conditions, with biodiesel exhibiting improved performance in colder climates when the biodiesel proportion is reduced. Conversely, biodiesel offers numerous benefits, including ease of use, a reduction in pollution and reliance on foreign oil, lower toxicity, and simpler storage compared to petroleum[6]. The biodiesel production industry has consistently expanded as a viable alternative to petroleum consumption. High-cost production presents a significant challenge, primarily due to the expensive biodiesel feedstock and the purification process involved. Additionally, soap formation may take place if an excess of catalyst is employed when utilizing a homogeneous catalyst, owing to its sensitivity to water and free fatty acids. This will result in a low yield of biodiesel and lead to issues during product purification, as it requires a significant amount of water. Therefore, this study will emphasize the utilization of more economical and waste feedstock derived from palm fatty acid distillate (PFAD), along with the development of various metal oxides supported on hydroxyapatite (HAP) catalysts.

Materials

Palm fatty acid distillate (PFAD) which is a feedstock for biodiesel production retrieved from Sarawak Palm Oil Berhad. Calcium nitrate tetrahydrate ($Ca(NO_3)_2.4H_2O$) and ammonium dihydrogen phosphate ($NH_4H_2PO_4$) from R&M Chemicals, magnesium nitrate ($Mg(NO_3)_2.6H_2O$) and copper II sulphate ($CuSO_4.5H_2O$) from Systerm, sodium nitrate ($NaNO_3$) from Fluka, hydrochloric acid (HCl) from Sigma-Aldrich, sulfuric acid (H_2SO_4) from J.T.Baker, ethanol from Systerm, methanol from HmbG Chemicals, potassium hydroxide (KOH) from J.T.Baker, standard of myristate, palmitate, stearate, oleic, linoleic, methyl heptadecanoate and n-hexane from Sigma-Aldrich. Ethanolic potassium hydroxide was prepared in the laboratory by dissolving potassium hydroxide in ethanol. 3% Ammonia solution was prepared by diluting 30% ammonia solution with distilled water.

Catalyst preparation

Calcium nitrate tetrahydrate and ammonium dihydrogen phosphate were weighed 15.08 g and 5.08 g, respectively and were put in different conical flask label as A (calcium nitrate tetrahydrate) and B (ammonium dihydrogen phosphate). Then, both was diluted with 160 mL of distilled water and 3% ammonia solution was dropwise to adjust the pH 10–11. Solution A was put in round bottom flask and mixture solution B was put into burette and was dropwise into solution A while stirring. Then, the mixed solution was refluxed in fume hood for 2 h at 90 °C. The liquid samples were centrifuged for 5 min at 350 rpm and left to dried in oven overnight. The dried samples (solid) then were grinded and calcined using air furnace for 4 h at 400 °C. This solid samples been labelled as HAP support. Next, the obtained HAP and $NaNO_3$ were weighed and added together in the beaker. Then, the metal salt were then added to solution and stirred for 2 h. After that, the mixtures was dried in oven overnight. The sample then was grinded and calcined using furnace for 4 h at 400 °C under atmosphere condition. The same steps were repeated using Cu_2SO_4 and $Mg(NO_3)_2$. All the catalyst were then sulfonated with H_2SO_4 while stirring overnight. Then, the solution were rinsed using distilled water, filtered and dried in oven.

Catalyst characterization

The crystallography of the AC catalysts doped with the mixed oxide was investigated via the x-ray diffraction (XRD) technique. The x-ray diffraction (XRD) was conducted with a Shimadzu diffractometer (Model XRD-6000). The BET surface area and pore size distributions of the catalysts were investigated with a Brunauer-Emmet-Teller (BET) adsorption/desorption analyser using nitrogen gas (N2). Prior to BET analysis, the catalysts were degassed at 150 °C for 24 h to remove all moisture and volatile impurities from the surface of the catalysts. Nitrogen gas was used as both adsorbent and desorbed in a vacuum chamber at − 196 °C. Additionally, the acid properties of the catalysts were evaluated using temperature-programmed desorption (TPD) with ammonia (NH3) as a probe molecule. A TPD/R/O 1100 (Thermo Finnigan) with a Thermal Conductivity Detector (TCD) was utilized for this study. The catalyst (approximately 0.05 g) was initially treated with a flow of nitrogen gas at 250 °C for 30 min. After treatment with nitrogen gas, the catalyst was exposed to ammonia gas at room temperature for one hour to allow ammonia to adsorb onto the surface of the catalyst. All excess ammonia was removed from the surface of the catalyst with a flow of nitrogen gas. The ammonia that had adsorbed onto the surface of the catalyst during exposure to ammonia gas was desorbed into a helium flow (30mL/minute) and monitored with the TCD from 50 °C to 950 °C with a hold time of 30 min at each temperature. Thermogravimetric analysis (TGA) of the catalysts was also performed utilizing a TGA (Mettler Toledo 990). Finally, the chemical functional groups of the biodiesel products formed during transesterification reactions were characterized using Fourier Transform Infrared Spectroscopy (FTIR) and a Perkin Elmer Spectrum (PS) Spectrum 100 FTIR spectrometer with a resolution of 4 cm − 1 over a wave number range of 300–4000 cm − 1.

Transesterification reaction

0.3 g of catalyst metal/HAP prepared was weighed and put into round bottom flask. 16.5mL of methanol and 10 g of PFAD (ratio 10:1 methanol: oil) was added and then, it was refluxed for 2 h at 65 °C while stirring. The

oil mixture then was centrifuged for 10 min at 350 rpm. Then, it was stirred for 1 h at 70 °C. The oil sample then titrated with 0.5 M KOH to find the acid value.

Catalyst characterization

XRD

X-ray diffraction (XRD) analysis was conducted on the calcined catalysts over a 2θ range of 20°–80° for phase identification, referencing the International Centre for Diffraction Data (ICDD). As illustrated in Fig. 1, all catalysts exhibited characteristic diffraction peaks corresponding to the hydroxyapatite (HAP) phase at 2θ values of 26.0°, 32.2°, 34.2°, 39.8°, 46.7°, 49.5°, 53.4° and 64.3° (ICDD Card No.: 00-01-1008). These results confirm the successful synthesis of highly crystalline HAP at the selected calcination temperature, demonstrated by the presence of well-defined and intense peaks exclusively attributed to the HAP phase[7]. This indicates that the calcination process effectively converted the precursor materials into pure HAP, with negligible formation of secondary phases such as β-tricalcium phosphate (β-TCP) or monetite, which commonly arise at higher temperatures or under suboptimal conditions[8].

In addition to the primary hydroxyapatite phase, the XRD examination of Cu/HAP catalyst shows clear monoclinic tenorite (CuO) (ICDD Card No.: 00-002-1041) at 2θ: 32.2°, 38.9°, 47.1°, 48.9°, 65.9° and 67.2° and copper oxide sulfate, Cu_2O_5S (ICDD Card No.: 00-011-0196) at 2θ : 28.7°, 31.6°, 32.2°, 38.9°, 45.7°, 47.1°, 48.9°, 52.5°, 56.0°, 59.3°, 61.0°, 65.9° and 67.2°. These stages imply improved acidity and redox characteristics, which may influence stability but may also increase catalytic activity. Meanwhile Na/HAP shows existence of orthorhombic sodium oxide (Na_2O) (ICDD Card No.: 00-006-0500), and rhombohedral magnesium oxide (MgO) (ICDD Card No.: 00-027-0759), which probably improve structural robustness and surface basicity. The addition of these metals significantly increased the intensity of the HAP peak at 2θ = 32.2°. Among the catalysts, the Cu/HAP catalyst displayed a more pronounced and sharper peak at this position, whereas the Mg/HAP and Na/HAP catalysts presented broader and less strong peaks. This disparity indicates that Cu/HAP catalyst exhibits superior crystallinity and increased crystallite size, which likely replace copper ions in the lattice owing to their analogous ionic radii, hence facilitating lattice ordering and crystal development during calcination[9]. Conversely, Mg/HAP and Na/HAP exhibit reduced crystallite sizes and diminished crystallinity owing to lattice distortions caused by variations in ionic size and charge, which may impede crystal development and lower crystallinity[10,1]. Consequently, this structural advantage likely enhances the performance of Cu/HAP in biodiesel production relative to Mg/HAP and Na/HAP catalysts. The crystal size where calculated as 10.4 < 13.9 < 45< 52.8 nm for the HAP, Na/HAP, Mg/HAP and Cu/HAP respectively.

XPS analysis

The surface chemical states of the modified hydroxyapatite catalysts were examined by high-resolution X-ray photoelectron spectroscopy (XPS), focusing on the Na 1s, Mg 2p, and Cu 2p core levels. For the Na/HAP catalyst, the Na 1s spectrum exhibits a single, symmetric peak centered at approximately 1071.0–1071.3 eV, which is characteristic of Na^+ species in an ionic environment. This binding energy is consistent with sodium coordinated to oxygen atoms, such as Na–O or Na–O–P linkages, indicating that Na is successfully incorporated on the HAP surface, most likely through partial substitution of Ca^{2+} sites and/or electrostatic interaction with

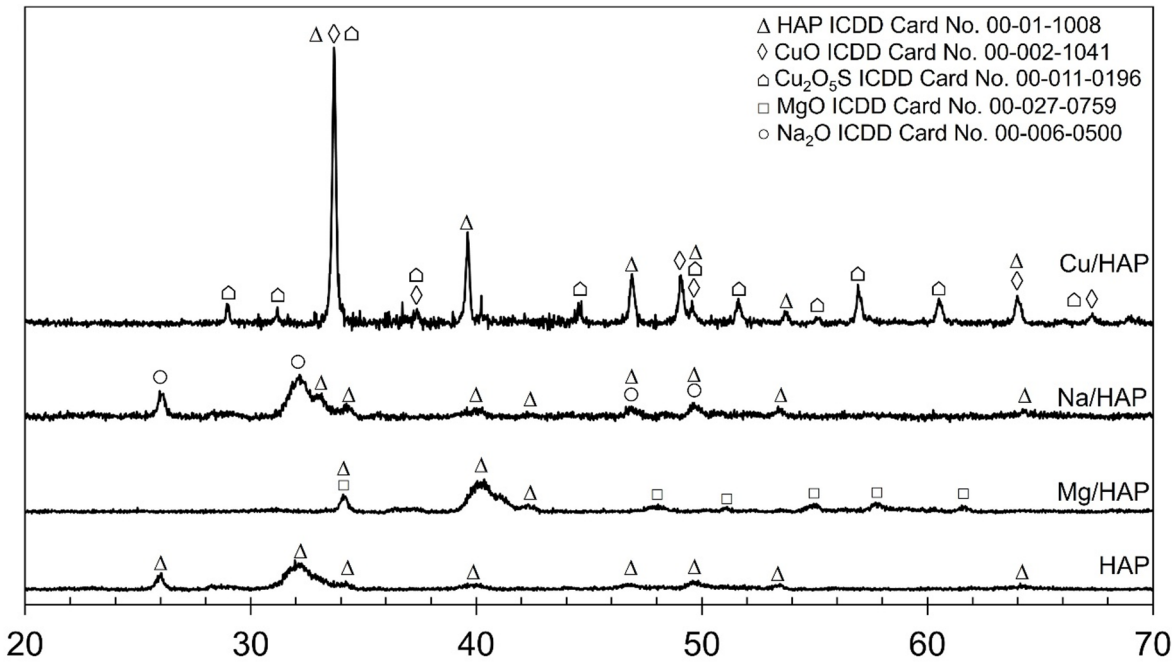

Fig. 1. XRD pattern for HAP, Cu/HAP, Mg/HAP and Na/HAP catalysts.

surface phosphate (PO_4^{3-}) and hydroxyl (OH^-) groups. The relatively higher Na 1s intensity compared to the other samples confirms a higher surface concentration of sodium in the Na-modified catalyst.

The Mg 2p spectrum of the Mg/HAP catalyst shows a dominant peak located at around 49.8–50.2 eV, which is typical of Mg^{2+} species bonded to oxygen. This binding energy corresponds to Mg–O and Mg–O–P environments, suggesting that magnesium is present in an oxidized state and strongly anchored to the hydroxyapatite matrix. Minor higher-binding-energy contributions extending toward ~51–52 eV can be attributed to Mg^{2+} species in slightly different coordination environments, such as more strongly interacting surface Mg–O–P sites or partially substituted Mg within the HAP lattice. These results confirm the successful incorporation of Mg into the HAP structure and its stabilization through strong metal–support interactions.

For the Cu/HAP catalyst, the Cu 2p region is characterized by two well-defined peaks at approximately 933–934 eV and 953–954 eV, corresponding to the Cu $2p_3/_2$ and Cu $2p_1/_2$ spin–orbit components, respectively. In addition, a broad shake-up satellite feature is observed in the 940–945 eV region, which is a diagnostic signature of Cu^{2+} species. The presence of these satellite peaks, together with the binding energy position of the main Cu $2p_3/_2$ peak, confirms that copper is predominantly present in the oxidized Cu^{2+} state rather than as Cu^0 or Cu^+. This indicates strong interaction of Cu species with the oxygen-containing functional groups of hydroxyapatite, forming Cu–O, Cu–OH, or Cu–O–P surface species. Overall, the XPS results demonstrate that Na, Mg, and Cu are successfully incorporated onto the HAP surface in their respective ionic states, with strong metal–support interactions that are expected to play a crucial role in determining the catalytic behavior of the modified HAP catalysts.

TGA

The catalysts' thermogravimetric analysis (TGA) showed notable thermal deterioration characteristics in the Na/HAP, Mg/HAP, and Cu/HAP catalysts, which are presented in Fig. 2. Na/HAP and Mg/HAP exhibited two distinct stages of weight loss, whereas Cu/HAP displayed only a single weight-loss event. The initial weight loss observed above 100 °C in all three catalysts primarily results from the removal of physically adsorbed and structural water, consistent with previous findings that highlight water desorption and dehydration of hydroxyapatite occurring below 200 °C [12]. A secondary weight loss of approximately 5% and 3% was observed for Na/HAP and Mg/HAP, respectively, at temperatures exceeding 500 °C. This advanced stage involves the decomposition of residual organic matter in the composite, which includes nitrate species and other organic contaminants. This is supported by prior findings mentioning specifically regarding the breakdown of sodium nitrate ($NaNO_3$) in relation to Na/HAP[13,14]. The presence of this secondary breakdown phase indicates insufficient removal or integration of dopant-related entities, which could affect the stability of the catalyst. In contrast, Cu/HAP demonstrated improved thermal stability, with only the initial weight reduction associated with water evaporation and no significant mass loss at higher temperatures. The enhanced stability arises from the sulfonation process, which strengthens the binding of copper ions to the HAP surface, consequently reducing labile organic residues and improving the catalyst's thermal resilience. The ability of Cu/HAP to maintain structural integrity at elevated temperatures underscores the effectiveness of sulfonation in enhancing metal-support interactions and suggests its potential advantages in catalytic applications that require thermal stability (Fig. 3).

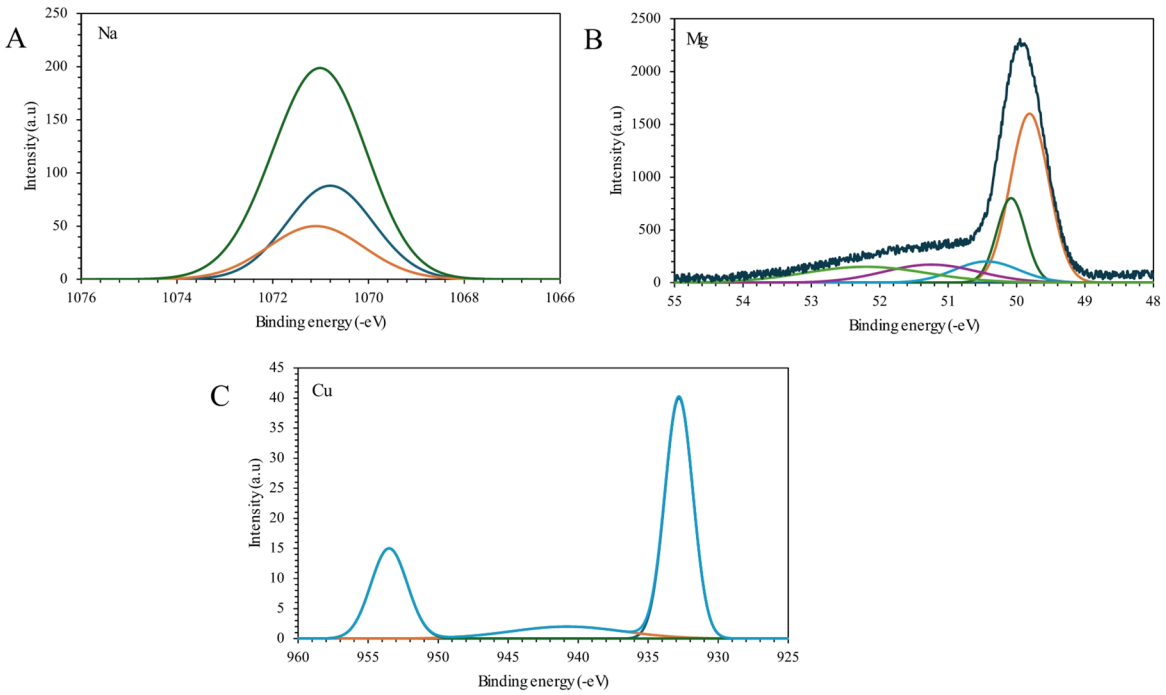

Fig. 2. XPS analysis for Na/HAP, Mg/HAP, and Cu/HAP.

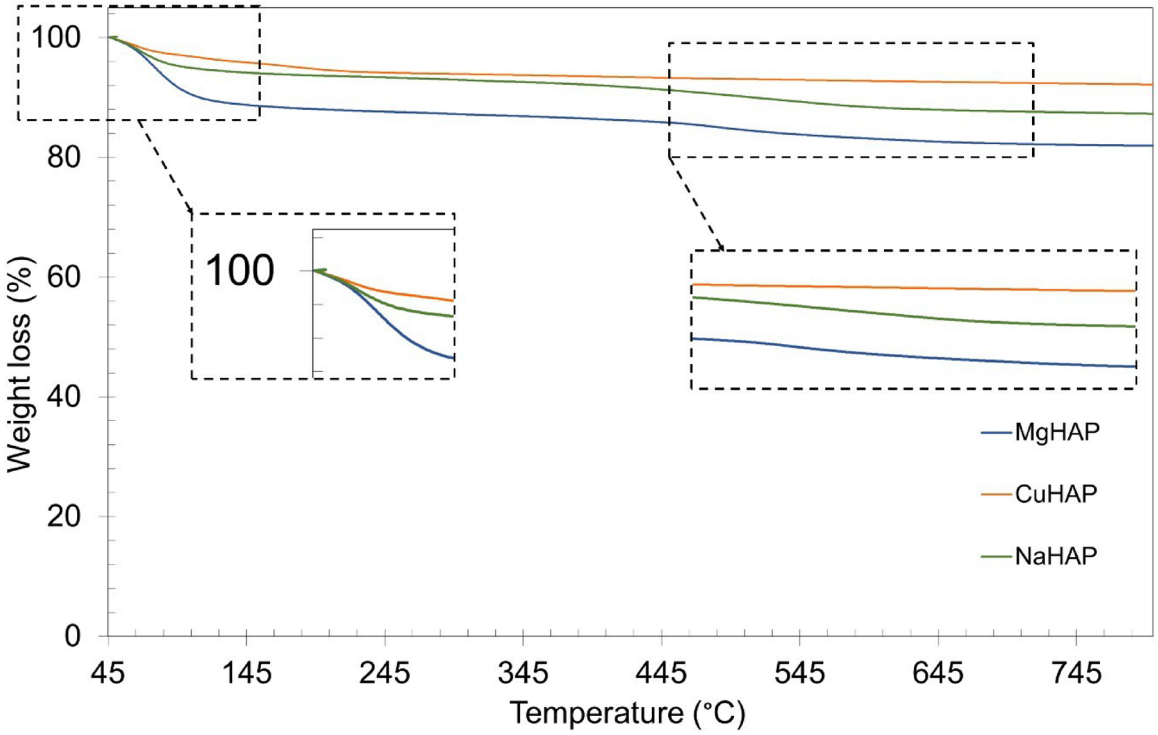

Fig. 3. Thermogravimetric profiles of Cu/HAP, Mg/HAP and Na/HAP catalysts.

BET

The Cu/HAP catalyst, according to the IUPAC classification system, exhibits type IV nitrogen adsorption-desorption isotherms with an H3 hysteresis loop, which is characteristic of mesoporous materials[15]. The mesoporous characteristics are clearly depicted in Fig. 4A, where the isotherm shape and hysteresis loop confirm the presence of slit-shaped pores typically associated with aggregates of plate-like particles or non-rigid pore networks[16]. The sulfonation treatment of the catalyst influences its textural properties by modifying the pore structure, particularly leading to a decrease in pore volume and width. Prior researcher showed that sulfonation may lead to partial pore blockage or narrowing as a result of sulfonic acid groups being incorporated on the catalyst surface[17]. This modification enhances the acidity of the catalyst, albeit with a slight decrease in pore capacity, thereby optimizing the diffusion of reactants and their accessibility to active sites. Figure 4B illustrates that the Cu/HAP catalyst has a significant average pore diameter of approximately 100 nm, placing it in the mesoporous category (2–50 nm according to IUPAC, though some sources extend mesoporosity to 100 nm). This indicates the presence of wide mesopores that facilitate the mass transfer of larger molecules such as triglycerides found in feedstocks. The Brunauer–Emmett–Teller (BET) surface area of Cu/HAP is measured at 1.0 m^2/g, with a pore volume of 0.000868 cm^3/g. Although these values are relatively low, they are sufficient to provide accessible active sites for catalytic processes. The relationship between mesoporosity and surface area is crucial for catalytic performance, as it enhances the diffusion of reactants and products, thereby improving catalytic efficiency. The structural advantage is particularly relevant for biodiesel production from palm fatty acid distillate (PFAD), as the mesoporous properties of Cu/HAP can accommodate larger molecules and improve conversion efficiency. It was also been discovered that catalysts with higher BET surface areas and mesoporous structures demonstrate improved catalytic activity in the production of fatty acid methyl esters (FAME) from soybean oil, underscoring the importance of these textural features[18]. Previous research also emphasized that pore widths ranging from 2 to 10 nm are categorized as ultrafine mesopores, enhancing catalytic efficiency by increasing the number of accessible active sites[19]. The findings suggest that the mesoporous structure of Cu/HAP, combined with its tailored surface chemistry through sulfonation, plays a vital role in improving its catalytic effectiveness for biodiesel production. This enhancement leads to better access for reactants, increased exposure of active sites, and improved overall reaction kinetics.

TPD-NH_3

The NH_3-TPD study illustrated in Fig. 5 shows two notable desorption peaks at approximately 700 °C and 900 °C, suggesting the presence of strong acid sites on the Cu/HAP catalyst. The acidic sites are classified based on their desorption temperatures, with those exceeding 500 °C considered strong, while sites with lower temperatures are identified as having moderate or weak acidity[20]. Strong acid sites are significantly present in the large areas below these peaks, which are measured at 421.9 µmol/g and 1711.7 µmol/g, respectively. This is corroborated by earlier studies that highlighted the connection between peak area and acid site density[21]. Strong acid sites arise from sulfonic acid groups formed during the sulfonation process, imparting considerable Brønsted acidity to

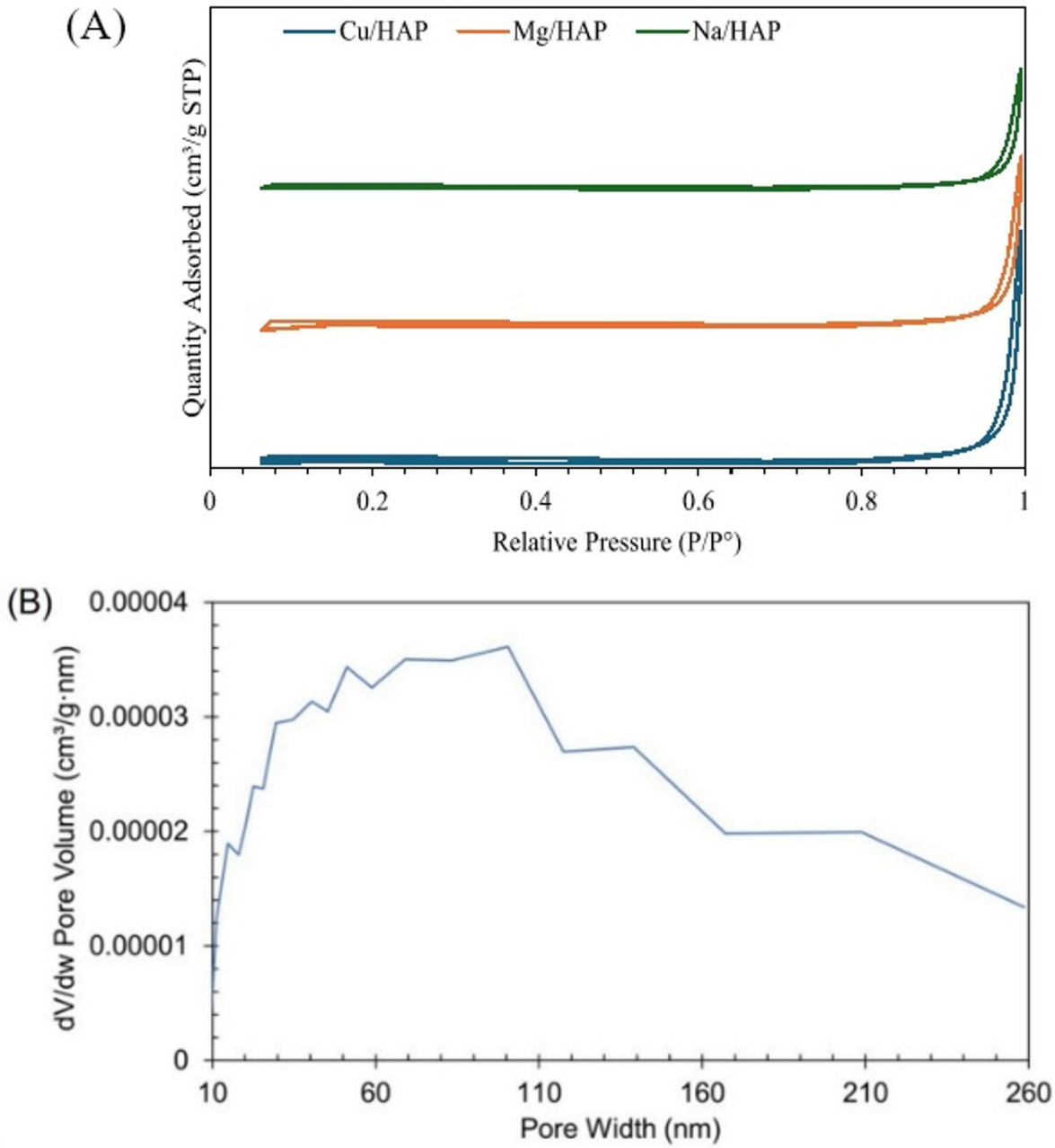

Fig. 4. (**A**) Nitrogen adsorption isotherm (BET) and (**B**) BJH pore size distribution of Cu/HAP catalyst.

the catalyst surface[17,22]. The presence of Brønsted acid sites plays a vital role in the esterification of palm fatty acid distillate (PFAD), acting as proton donors that enhance the conversion of free fatty acids into biodiesel by facilitating reaction kinetics[23]. The strong acid sites, along with the mesoporous structure and adequate surface area of Cu/HAP, facilitate optimal access for reactants to the active sites and improve catalytic performance. The relationship between the catalyst's textural features and its high concentration of strong acid sites confirms its suitability and effectiveness for biodiesel production from PFAD. The acidity strength were Cu/HAP > Mg/HAP > Na/HAP.

Liquid product characterizations

Acid value and FFA conversion

The FFA conversion data in Fig. 6; Table 1 reveal that the Cu/HAP catalyst achieved the highest conversion rate of 61.2%, while Na/HAP showed the lowest rate at 21.8%. The Na/HAP demonstrated the highest acid value, suggesting its insufficient effectiveness in the conversion of PFAD to biodiesel. The main reason is that Na/HAP functions as a highly basic catalyst, whereas PFAD acts as a feedstock with a high free fatty acid content. Under these conditions, basic catalysts are prone to saponification, leading to soap formation rather than esterification, which significantly reduces biodiesel yield and catalyst efficiency. This observation is consistent with the earlier

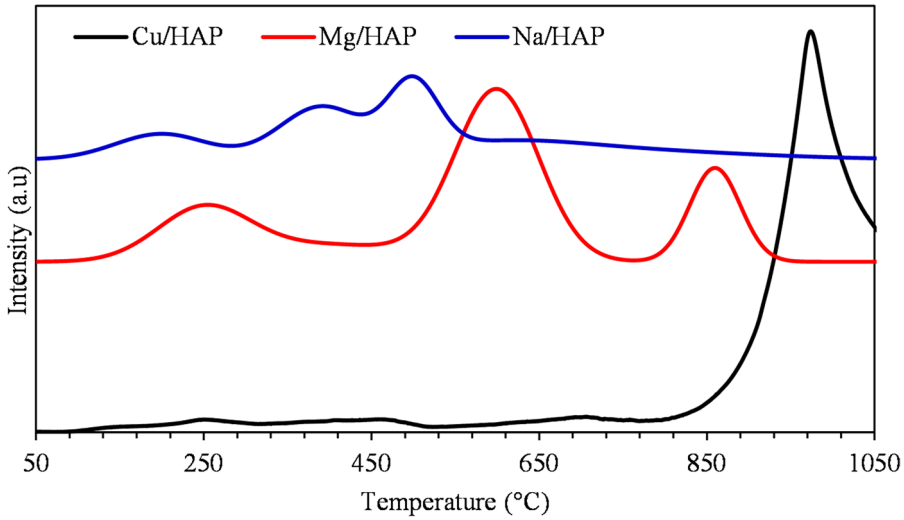

Fig. 5. Acidity Profile of Cu/HAP, Mg/HAP and NaHAP Catalyst via TPD-NH_3.

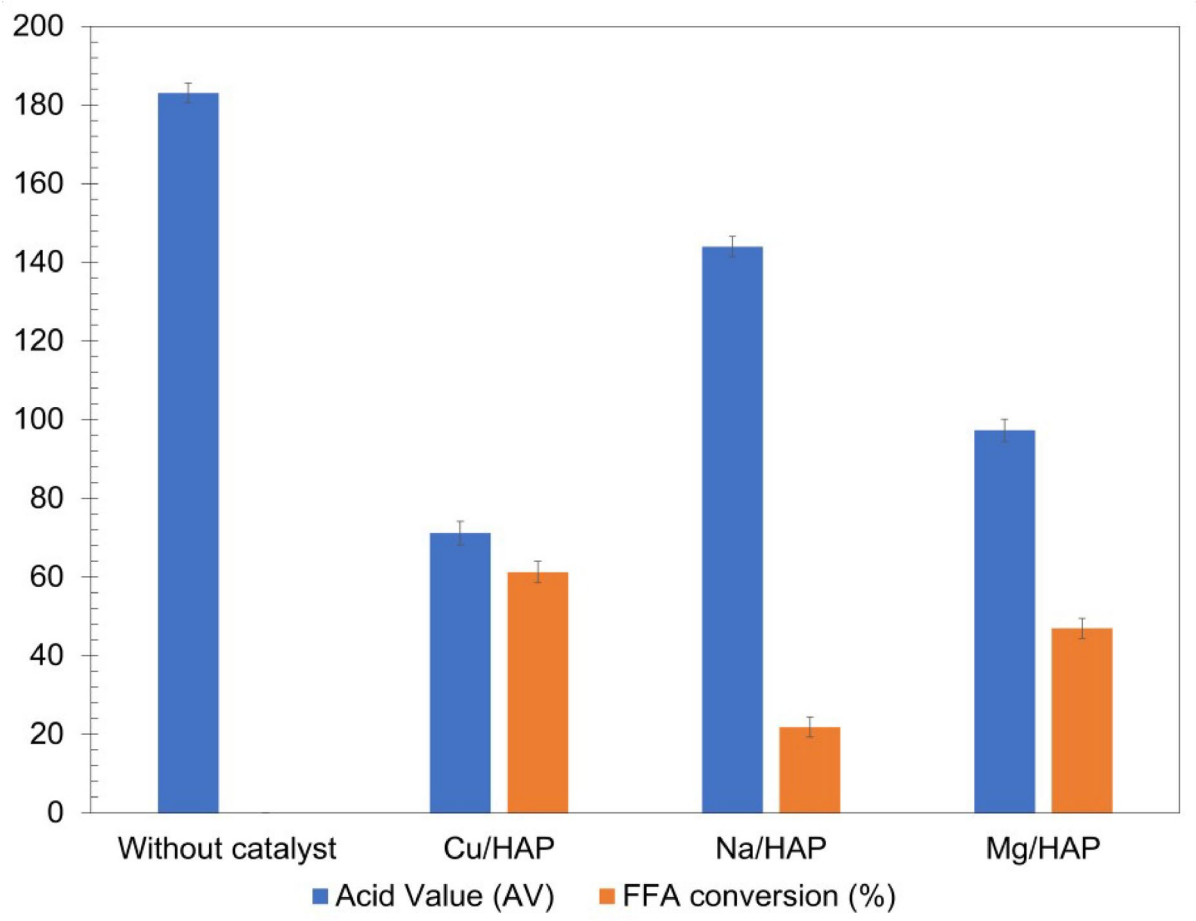

Fig. 6. Acid value and FFA conversion profiles for blank and HAP-catalyzed reactions on PFAD.

investigation indicated that base catalysts are unsuitable for high-FFA feedstocks due to their tendency to promote saponification[24]. The Cu/HAP catalyst demonstrated exceptional performance, reaching an acid value of 71.11 and an FFA conversion of 61.2% (Table 1). Sulfonation with sulfuric acid enhances the acidic characteristics of the Cu/HAP catalyst, increasing the density of strong Brønsted acid sites on the catalyst surface and contributing to its better performance. By encouraging esterification processes and inhibiting saponification, Cu/HAP

Metal catalyst	Acid value (AV)	FFA value	FFA conversion (%)
Without catalyst	183.04	91.52	–
Na/HAP	71.11	35.56	61.2
Cu/HAP	143.94	71.97	21.8
Mg/HAP	97.23	48.62	46.9

Table 1. Comparison value of acid and FFA value on the blank and HAP-based catalyst.

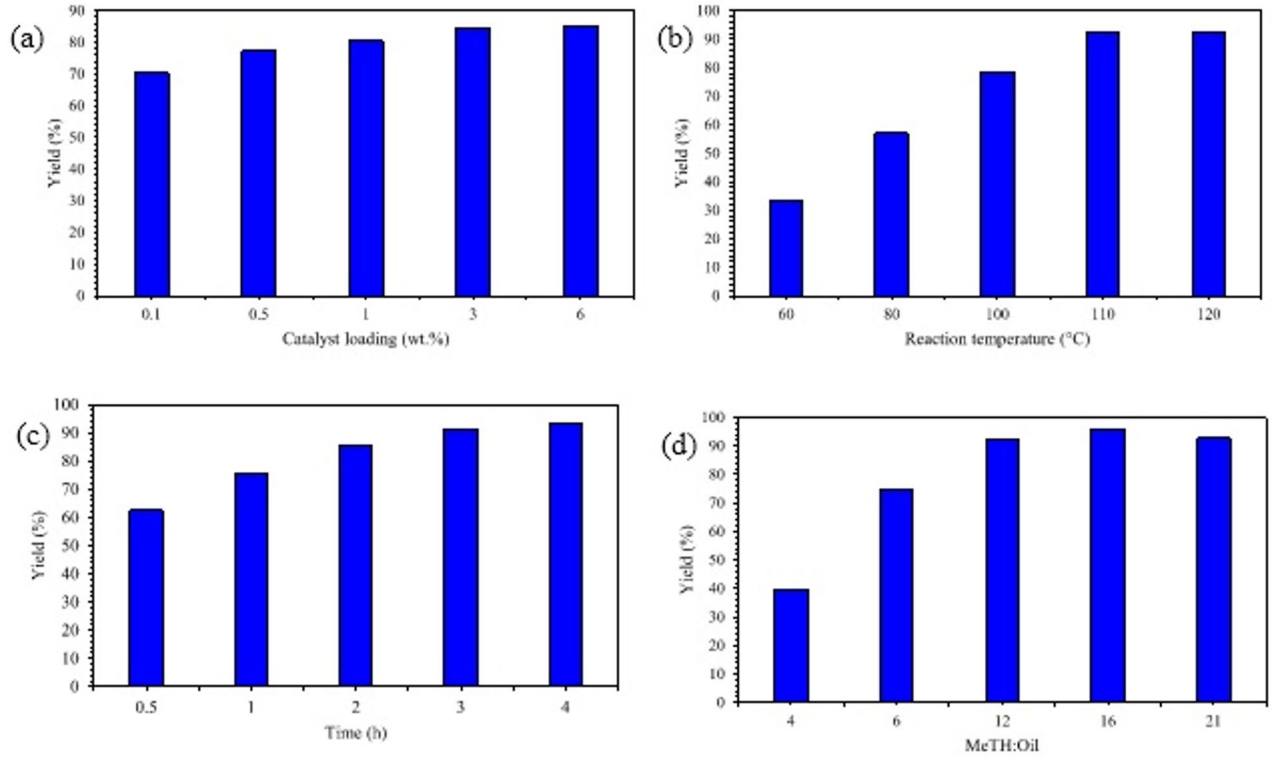

Fig. 7. Influence of key process parameters on biodiesel yield: (**a**) effect of reaction temperature on transesterification efficiency, (**b**) variation of biodiesel yield with alcohol-to-oil molar ratio, (**c**) impact of catalyst concentration on ester formation, and (**d**) effect of reaction time on biodiesel yield. The trends highlight the existence of optimal operating conditions governed by reaction kinetics, equilibrium limitations, and phase separation behavior.

effectively acts as an acid catalyst for high-FFA feedstocks, increasing the output and purity of biodiesel. Earlier studies highlighting the preference for acid catalysts in these applications[25,26]. Despite being the highest of the catalysts evaluated, the FFA conversion for Cu/HAP is still below the theoretical limit. The noted discrepancy could stem from experimental variables, such as water contamination from the condenser during the reaction, which may promote soap formation and hinder the conversion of triglycerides to biodiesel. Prior study also demonstrated that the presence of water in high-FFA systems can enhance saponification, which in turn reduces the efficiency of the catalyst and the yield of biodiesel[27]. The findings emphasize the importance of utilizing acid catalysts like sulfonated Cu/HAP for high-FFA feedstocks and the critical need for precise control over reaction conditions to enhance conversion and minimize side reactions.

Reaction optimization

Figure 7(a) illustrates the effect of reaction temperature on biodiesel yield under otherwise fixed operating conditions. As shown in the figure, the biodiesel yield increases steadily with increasing temperature, indicating enhanced transesterification kinetics and improved miscibility between the oil and alcohol phases. At lower temperatures, limited molecular motion and higher oil viscosity restrict effective contact between reactants, resulting in incomplete conversion. The maximum biodiesel yield is achieved within an intermediate temperature range, beyond which further temperature increase leads to yield stabilization or a slight decline. This behavior can be attributed to alcohol evaporation, reduction in effective reactant concentration, and the possible onset of thermal degradation or reverse reactions, demonstrating that temperature optimization is essential to maximize yield while preserving reaction stability.

Figure 7(b) presents the influence of the alcohol-to-oil molar ratio on biodiesel yield. The figure shows a pronounced increase in yield with increasing molar ratio up to an optimum value, consistent with equilibrium-driven enhancement of ester formation. Higher alcohol availability facilitates the forward transesterification reaction and improves triglyceride conversion. However, further increases in the molar ratio result in a marginal improvement or reduction in biodiesel yield. This decline is mainly due to excessive alcohol dissolving glycerol into the ester phase, which disrupts phase separation and reduces apparent yield. The results indicate that excessive alcohol addition is counterproductive despite its favorable effect on reaction equilibrium.

The effect of catalyst concentration on biodiesel yield is depicted in Fig. 7 (c). At low catalyst loading, the biodiesel yield remains relatively low due to insufficient active sites available for triglyceride conversion. Increasing catalyst concentration enhances reaction rates and promotes ester formation, leading to a sharp rise in biodiesel yield. An optimum catalyst concentration is clearly observed, corresponding to maximum yield. Beyond this optimum, the yield either plateaus or decreases slightly, which can be attributed to soap formation, increased mixture viscosity, and emulsification phenomena. These effects hinder effective biodiesel–glycerol separation and reduce product recovery efficiency, highlighting the importance of maintaining an optimal catalyst dosage.

Figure 7(d) shows the effect of reaction time on biodiesel yield. The biodiesel yield increases rapidly during the initial stages of the reaction, reflecting progressive triglyceride conversion toward fatty acid methyl esters. As reaction time increases, the yield approaches a maximum value, indicating that the system has reached near-equilibrium conditions. Extending the reaction time beyond this point does not produce a significant improvement in yield and may even cause a slight decrease due to ester hydrolysis or backward reactions. From a process optimization perspective, this confirms that prolonged reaction times are energetically inefficient and unnecessary once equilibrium conversion is achieved.

Overall, Figs. 7(a–d) collectively demonstrate that biodiesel yield is controlled by a complex interplay of thermal effects, reaction equilibrium, catalytic activity, and time-dependent conversion behavior. The optimized operating conditions identified from these experimental trends ensure maximum biodiesel yield while avoiding kinetic limitations, excessive reagent usage, and separation challenges. These results confirm that reliable process optimization can be achieved through systematic experimental analysis, providing a solid foundation for scale-up and industrial application of biodiesel production.

GC-FID

The GC-FID analysis (see Fig. 8 **and** Table 2) confirmed the successful production of biodiesel, primarily composed of five fatty acid methyl esters (FAMEs): methyl myristate (C14:0), methyl palmitate (C16:0), methyl stearate (C18:0), methyl oleate (C18:1), and methyl linoleate (C18:2) [28]. The total biodiesel yield was found to

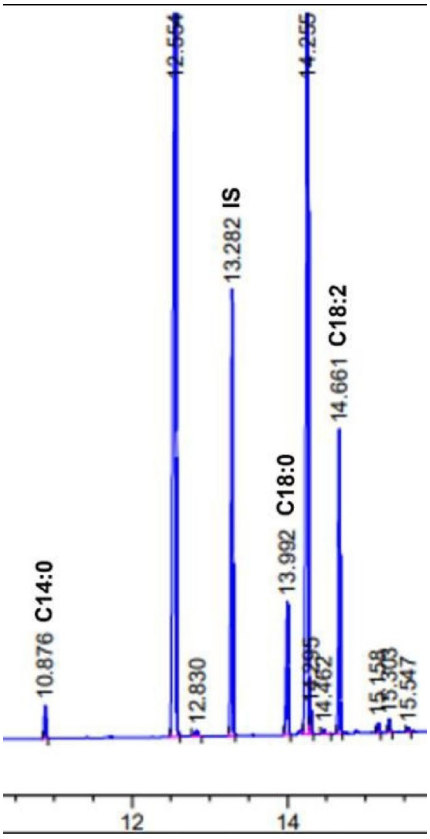

Fig. 8. GC-FID spectrum showing FAMEs in Cu/HAP-catalyzed liquid product.

FAME	Yield (%)
Methyl myristate (C14:0)	2.70
Methyl palmitate (C16:0)	43.22
Methyl stearate (C18:0)	37.89
Methyl oleate (C18:1)	10.40
Methyl linoleate (C18:2)	3.78
Others	2.01

Table 2. The FAME combustion of the biodiesel product.

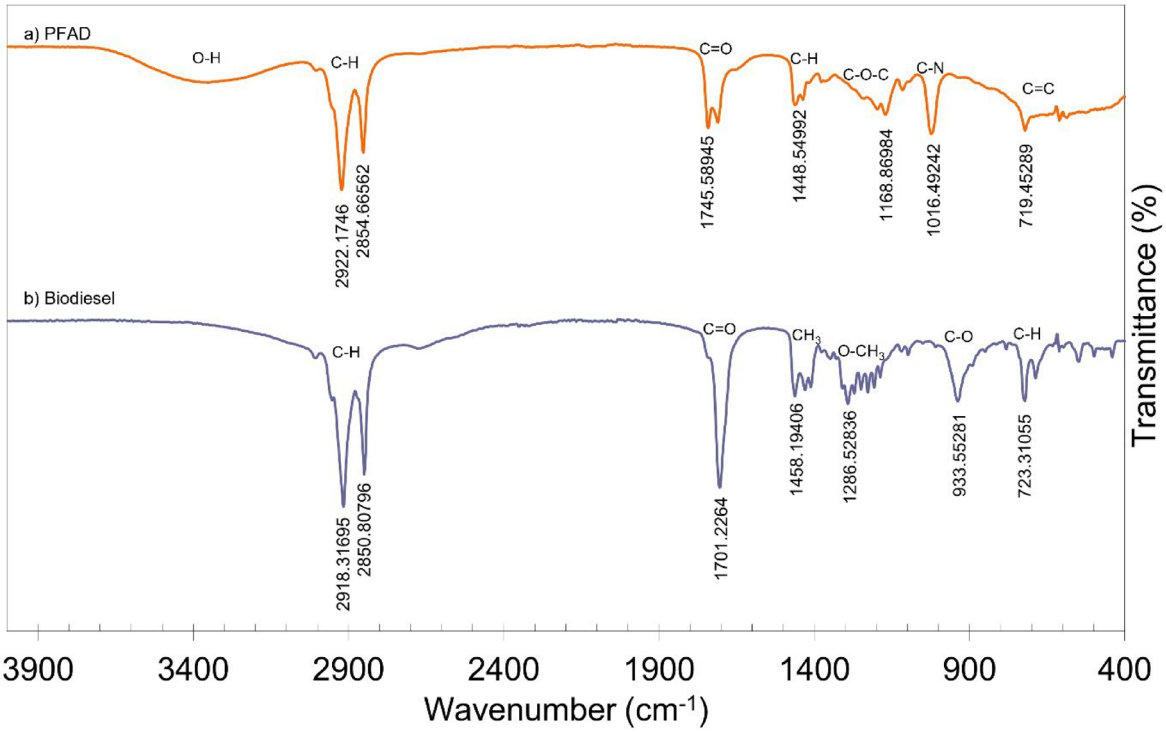

Fig. 9. FTIR Spectra of PFAD feedstock and biodiesel produced using Cu/HAP catalyst.

be 40.4% using standard GC-FID quantification methods, which rely on the relationship between peak area and component concentration. The elution sequence of these methyl esters followed an ascending order of carbon numbers, from C14:0 to C18:2, consistent with established chromatographic principles. FAMEs with longer chains and higher levels of unsaturation eluted later due to increased polarity and molecular weight. Methyl palmitate (C16:0) and methyl oleate (C18:1) exhibited the largest peak areas, indicating their higher concentrations in the biodiesel sample, while methyl myristate, methyl stearate, and methyl linoleate were found in smaller amounts, as evidenced by their reduced peak areas. This range is typical of biodiesel produced from common vegetable oils and aligns with previous research on FAME profiling using GC-FID[28,29]. The clear identification of the five main methyl esters, based on retention times and peak integration, demonstrates the effectiveness of the transesterification process and the suitability of GC-FID for assessing biodiesel quality[30]. The findings confirm that the catalytic system successfully facilitated the conversion of PFAD into biodiesel, exhibiting a distinct FAME profile, highlighting its potential for practical biodiesel production.

FTIR

FTIR Fourier transform infrared spectroscopy (FTIR) was employed to monitor the progress of the transesterification reaction of palm fatty acid distillate (PFAD) catalyzed by Cu/HAP. According to its acidic catalytic properties, only Cu/HAP demonstrated an efficient conversion of PFAD to biodiesel among the catalysts tested. On the other hand, under the given reaction conditions, the basic catalysts Na/HAP and Mg/HAP showed no discernible activity. The FTIR spectrum of PFAD (Fig. 9) reveals clear absorption bands linked to various functional groups. The interval from 600 to 750 cm^{-1} corresponds to the bending vibrations of C = C bonds found in alkene groups. The region between 900 and 1000 cm^{-1} is associated with C–N stretching from fatty amide groups. The stretching vibrations of C–O–C occur within the range of 1100–1300 cm^{-1}. The bending of C–H bonds in alkanes is observed in the range of 1400–1500 cm^{-1}. The prominent carbonyl (C = O) stretch

of carboxylic acids is detected within the range of 1650–1750 cm^{-1}. Distinct peaks in the 2800–3100 cm^{-1} range indicate C–H stretching, whereas a broad absorption band observed at 3000–3400 cm^{-1} is associated with O–H stretching of carboxylic acid groups. The FTIR spectrum of the biodiesel product (see Fig. 9) shows significant changes that suggest the formation of esters. The bending vibrations of C–H bonds in alkanes can be detected within the range of 700–800 cm^{-1}. The 900–1000 cm^{-1} region signifies the C–O stretching vibrations associated with ester groups connected to $–CH_2$. The bending vibrations of $O–CH_3$, characteristic of esters, are observed in the range of 1100–1200 cm^{-1}. The asymmetric bending of CH_3 is observed within the range of 1300–1500 cm^{-1}. An intense and distinct peak observed at 1700–1800 cm^{-1} is linked to the C = O stretching of ester carbonyl groups. Furthermore, pronounced C–H stretching absorptions from alkanes are observed in the range of 2800–2900 cm^{-1}. The carbonyl peak in PFAD at 1650–1750 cm^{-1} shifts to a higher wavenumber region (1700–1800 cm^{-1}) in the biodiesel spectrum, indicating the transformation of carboxylic acid groups into ester functionalities. The noted shift and the appearance of ester-specific bands validate the effective transesterification process and the production of biodiesel facilitated by Cu/HAP. The FTIR results offer molecular-level insights into the structural changes that take place during the reaction, underscoring the efficacy of the Cu/HAP catalyst in facilitating biodiesel synthesis from PFAD.

Reusability study

The reusability data (Fig. 10), the Cu/HAP catalyst demonstrated good catalytic stability for the conversion of PFAD to biodiesel under the optimum reaction conditions. The fresh catalyst achieved a high biodiesel yield of ≈ 95% in the first cycle, confirming the high activity of Cu active sites supported on hydroxyapatite. Upon reuse, a slight but progressive decline in yield was observed, with biodiesel yields decreasing to ≈ 94% in the second cycle,≈92% in the third cycle, and ≈ 90% after the fourth cycle. This gradual loss in activity is mainly attributed to surface fouling by glycerol, adsorption of unreacted PFAD species, and partial blockage of basic active sites during repeated transesterification reactions. Notably, regeneration of the spent catalyst by recalcination effectively restored most of its catalytic performance, indicating that the deactivation was largely reversible and associated with surface deposition rather than permanent structural damage. The relatively small reduction in yield over multiple cycles highlights the strong metal–support interaction between Cu species and the HAP matrix, which helps to suppress Cu leaching and preserve active site integrity. Overall, the reusability results confirm that the Cu/HAP catalyst possesses excellent regenerability and durability, supporting its practical applicability for sustainable biodiesel production from PFAD.

Comparison with previous work

Based on the comparative data summarized in the attached table, the current study clearly demonstrates a meaningful advancement in heterogeneous catalytic transesterification for biodiesel production (Table 3). Previous studies have predominantly relied on alkali-modified oxides, biochar-based catalysts, bifunctional acid–base systems, or enzyme-assisted catalysts, which generally require relatively mild temperatures (~ 60–65 °C), higher alcohol-to-oil ratios, longer reaction times, or complex catalyst synthesis routes to achieve biodiesel yields in the range of ~ 91–94%. In contrast, the Cu/HAP catalyst developed in the present work achieves a notably higher biodiesel yield of 95.84% using palm fatty acid distillate (PFAD), a low-cost and industrial by-product feedstock, under comparatively moderate and industrially relevant conditions (110 °C, 2 h, methanol-to-oil ratio of 16:1, and only 1 wt% catalyst loading). The novelty of this study lies in the synergistic integration of copper species with hydroxyapatite, which provides well-distributed active sites combining basicity and metal-assisted activation, enabling efficient conversion of high-free-fatty-acid PFAD without the need for dual catalysts, enzymatic systems, or continuous-flow configurations. Moreover, unlike many reported systems that depend on refined vegetable oils or require elaborate synthesis strategies, the present catalyst is prepared via a simple wet impregnation method, enhancing scalability and economic feasibility. Collectively, these features position the

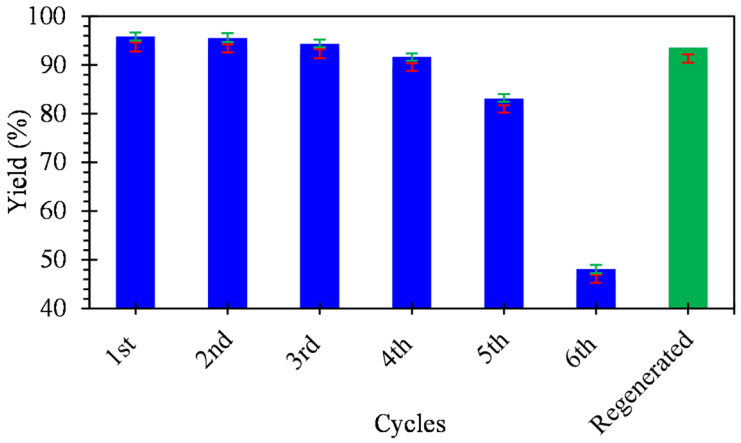

Fig. 10. Reusability and regeneration performance of the Cu/HAP catalyst for PFAD-to-biodiesel conversion under optimum reaction conditions, showing biodiesel yield over successive cycles.

Catalyst composition	Preparation method	Feedstock	Reaction conditions (T, time, alcohol-to-oil ratio, catalyst loading)	Biodiesel yield (%)	Reference
K-loaded mesoporous alumina (MA–K, 20–25 wt% K)	Sol–gel synthesis of mesoporous alumina using P123 template, followed by impregnation with KNO_3 and calcination	Vegetable oil	65 °C; 2 h; methanol-to-oil 12:1; catalyst loading not explicitly stated	92.2–94.4	Wu et al., *Advanced Powder Technology* (2014)
Activated carbon supported K catalyst (C1, 14.3 wt% K)	Carbonization of malt bagasse followed by KOH impregnation and calcination	Soybean oil	65 °C; 2 h; ethanol-to-oil 12:1; catalyst loading 10 wt% (catalyst/oil)	91.8 ± 1.0	Ali et al., *Renewable Energy* (2024)
ZnO-doped seaweed biochar (ZnO@Char)	Calcination of residual seaweed biomass to biochar, followed by ZnO deposition	Macroalgal oil (Gracilaria sp.)	61 °C; 120 min; methanol-to-oil 12:1; catalyst loading 3.9 wt%	92.04	Karthikeyan et al., *Energy Conversion and Management* (2026)
$ZrCl_4$/Ph-SBA-15 (acid) + polymer-supported NHC (base)	SBA-15 functionalization with $ZrCl_4$; synthesis of polymer-bound N-heterocyclic carbene; integrated continuous-flow system	Vegetable oils and animal fats	Continuous flow; residence time 2–4 h; methanol 30–40 equiv; catalyst loading not reported	93–96	Asadi et al., *Tetrahedron* (2016)
CalB@γ-CD-MOF/MXene	In-situ growth of γ-cyclodextrin MOF encapsulating Candida albicans lipase B, followed by MXene assembly	Vegetable oil (model oil)	Near-IR assisted; ~40–50 °C; methanol-to-oil not specified; enzyme-based catalyst	93.3	Ao et al., *Carbohydrate Polymers* (2024)
Cu/HAP	wet impregnation	Palm Fatty Acid Distillate (PFAD)	1 wt%; 110; 2 h and 1:16	95.84%	Current study

Table 3. Comparison with previous work.

Cu/HAP catalyst as a highly effective, sustainable, and industrially attractive alternative for biodiesel production, representing a clear improvement over previously reported catalytic systems.

Conclusion

This study methodically investigated the catalytic efficacy of metal-doped hydroxyapatite (HAP) catalysts—namely Mg/HAP, Na/HAP, and Cu/HAP—in the transesterification of palm fatty acid distillate (PFAD) to produce biodiesel. Of the synthesized catalysts, only sulfonated Cu/HAP exhibited notable catalytic activity, attaining a biodiesel yield of 40.4% under optimized reaction conditions. The exceptional performance of Cu/HAP is ascribed to its increased acidity, mesoporous architecture, and notable thermal stability, as validated by TGA, BET, and NH_3-TPD assessments. Conversely, basic catalysts (Mg/HAP and Na/HAP) proved inefficient owing to soap production and swift deactivation upon exposure to the elevated FFA level of PFAD. The results highlight the essential importance of acid-functionalization and metal-support interactions in creating effective catalysts for the efficient transformation of inexpensive, high-FFA feedstocks into biodiesel. This research provides significant insights into the design of heterogeneous catalysts for sustainable biofuel generation and underscores the promise of sulfonated Cu/HAP as a viable choice for industrial biodiesel applications.

Data availability

All the data that used in this research are a variable in the supplementary data.

Received: 28 June 2025; Accepted: 19 March 2026
Published online: 31 March 2026

References

1. Timilsina, B. (2020).
2. Shahzad, U. *Durreesamin J.*, **1**, 1–7. (2015).
3. Laura, E. Pence, chair, ACS Green Chemistry Institute Advisor, *C&EN Glob. Enterp.*, 100, 27–27. (2022).
4. Martinez-Guerra, E. & Gude, V. G. Assessment of sustainability indicators for biodiesel production. *Appl. Sci.* **7**, 869 (2017).
5. Ismail, S. A. A. & Ali, R. F. M. *Sci. Technol. Adv. Mater.*, **16**, 34602. (2015).
6. Firoz, S. *Int. Res. J. Eng. Technol.*, **4**, 530–533. (2017).
7. Mohamad Dom, A. H. et al. *J. Adv. Res. Micro Nano Eng.*, **23**, 115–127. (2024).
8. Kurzyk, A. et al. Biernat. Calcination and ion substitution improve physicochemical and biological properties of nanohydroxyapatite for bone tissue engineering applications. *Sci. Rep.* **13**, 1–17 (2023).
9. Noori, A. et al. Azami. Exploring the various effects of Cu doping in hydroxyapatite nanoparticle. *Sci. Rep.* **14**, 1–13 (2024).
10. Moseke, C., Gelinsky, M., Groll, J. & Gbureck, U. Chemical characterization of hydroxyapatite obtained by wet chemistry in the presence of V, Co, and Cu ions. *Mater. Sci. Eng. C Mater. Biol. Appl.* **33**, 1654–1661 (2013).
11. Bensalem, A., Kucukosman, O. K. & Raszkiewicz, J. Resultant effect of two different methods of incorporating metals in the hydroxyapatite structure on its mechanical properties. *J. Mech. Behav. Biomed. Mater.* **132**, 105301 (2022).
12. Jagadale, P. N., Jagtap, P. P., Joshi, M. G. & Bamane, S. R. *Adv. Mater. Lett.*, **7**, 325–329. (2016).
13. Essamlali, Y., Amadine, O., Larzek, M., Len, C. & Zahouily, M. Sodium modified hydroxyapatite: Highly efficient and stable solid-base catalyst for biodiesel production. *Energy Convers. Manag.* **149**, 355–367 (2017).
14. Monte, J. P., Fontes, A., Pereira, G. A. L. & Pereira, G. Santos. Preparation and characterization of Mg(II) doped hydroxyapatite biocomposites. *Results Chem.* **4**, 100625 (2022).
15. Thommes, M. et al. and K. S. W. Sing. Physisorption of gases, with special reference to the evaluation of surface area and pore size distribution (IUPAC Technical Report). *Pure Appl. Chem.*, 87, 1051–1069. (2015).
16. Amedlous, A. et al. Copper loaded hydroxyapatite nanoparticles as eco-friendly Fenton-like catalyst to effectively remove organic dyes. *J. Environ. Chem. Eng.* **9**, 105501 (2021).
17. Zailan, Z., Ali, H., Chau, J. W. & Jusoh, M. M. Tahir and Z. Y. Zakaria. *Chem Eng.*
18. Changmai, B., Sudarsanam, P. & Rokhum, S. L. Biodiesel production using a renewable mesoporous solid catalyst. *Ind. Crops Prod.* **145**, 111911 (2020).

19. Singh, R. P., Singh, J. P., Pal, A. & Kaur, T. Encapsulation of vancomycin in copper doped hydroxyapatite mesoporous nanoparticles of different morphologies. *J. Drug Deliv Sci. Technol.* **55**, 101441 (2020).
20. Torres, G. C., Manuale, D. L., Benítez, V. M. & Vera, C. R. Yori. Modification of the performance of WO3-ZrO2 catalysts by metal addition in hydrocarbon reactions. *Quim. Nova*. **35**, 748–754 (2012).
21. Zakaria, Z. Y. & Linnekoski, J. Amin. Catalyst screening for conversion of glycerol to light olefins. *Chem. Eng. J.* **207**, 803–813 (2012).
22. Deris, N. H., Rashid, U., Soltani, S., Choong, T. S. Y. & Nehdi, I. A. *Catalysts*, **10**, 638. (2020).
23. Akinfalabi, S. I., Rashid, U., Yunus, R. & Taufiq-Yap, Y. H. *Catalysts*, **9**, 184. (2019).
24. Dhawane, S. H. & Halder, G. *in Advances in Feedstock Conversion Technologies for Alternative Fuels and Bioproducts* pp. 199–220 (Elsevier, 2019).
25. Litinas, A. et al. *Biofuel Res. J.*, **7**, 1170–1177. (2020).
26. Vijayalakshmi, S., Anand, M. & Ranjitha, J. *in Microalgae cultivation for biofuels production* pp. 251–263 (Elsevier, 2020).
27. Atadashi, I. M., Aroua, M. K., Aziz, A. R. A. & Sulaiman, N. M. N. The effects of water on biodiesel production and refining technologies: A review. *Renew. Sustain. energy Rev.* **16**, 3456–3470 (2012).
28. Zhao, Z. et al. *Molecules*, https://doi.org/10.3390/molecules29153469
29. Ragonese, C., Tranchida, P. Q., Sciarrone, D. & Mondello, L. Conventional and fast gas chromatography analysis of biodiesel blends using an ionic liquid stationary phase. *J. Chromatogr. A*. **1216**, 8992–8997 (2009).
30. Tiyapongpattana, W., Wilairat, P. & Marriott, P. J. Characterization of biodiesel and biodiesel blends using comprehensive two-dimensional gas chromatography. *J. Sep. Sci.* **31**, 2640–2649 (2008).

Author contributions

Athirah Adzahar, Nur: Methodology, Investigation, Conceptualization, Validation, Writing-Original Draft preparation, Writing-Reviewing and Editing: Md Shahar, Syazana Amira: Methodology, Investigation: G. AbdulKareem-Alsultan: Methodology, Investigation; Naeemah A. Ibrahim; optimization study and Y.H. Taufiq-Yap: Funding.

Declarations

Competing interests

The authors declare no competing interests.

Additional information

Supplementary Information The online version contains supplementary material available at https://doi.org/10.1038/s41598-026-45587-x.

Correspondence and requests for materials should be addressed to A.G.A.A. or T.Y.Y.H.

Reprints and permissions information is available at www.nature.com/reprints.

Publisher's note Springer Nature remains neutral with regard to jurisdictional claims in published maps and institutional affiliations.